Packing efficiency and accessible surface area of crumpled graphene

Steven W. Cranford and Markus J. Buehler*

Center for Materials Science and Engineering, Massachusetts Institute of Technology, 77 Massachusetts Avenue, Cambridge, Massachusetts, USA and

Department of Civil and Environmental Engineering, Laboratory of Atomistic and Molecular Mechanics, Massachusetts Institute of Technology, 77 Massachusetts Avenue, Room 1-235A&B, Cambridge, Massachusetts, 02139 USA

(Received 21 September 2011; published 22 November 2011)

Graphene holds promise as an ultracapacitor due to its high specific surface area and intrinsic capacitance. To exploit both, a maximum surface area must be accessible while the two-dimensional (2D) graphene is deformed to fill volume. Here, we study stable crumpled graphene sheets of different lengths, L, using full atomistic molecular dynamics (MD) and determine a fractal dimension of $D \cong 2.36 \pm 0.12$, indicating efficient spatial packing. Introduction of defects inducing a transition from membrane-like to amorphous carbon further enhances packing efficiency. Further, variation of self-adhesion energy indicates a predominant role in randomly folded graphene. We determine that approximately 60% of the specific surface area of graphene is solvent accessible once crumpled and can be tuned with applied compression and crumpling. We analyze the solvent accessible surface area (SASA) and approximate the upper bound of free crumpled graphene capacitance to ≈329 F/g. Once crumpled, the achievable capacitance is highly dependent on the confined volume.

DOI: 10.1103/PhysRevB.84.205451 PACS number(s): 61.48.Gh, 62.23.Kn, 64.60.al, 81.05.ue

I. INTRODUCTION

Monolayer graphene is a two-dimensional (2D) layer of sp^2-bonded carbon that has remarkable mechanical and electrical properties,[1,2] and one of the strongest materials tested in terms of elastic modulus (approaching 1 TPa) and tensile strength (>100 GPa).[1] Such superlative properties facilitate the design of advanced composites with superior mechanical and electrical performance.[3] Although graphene has an exceptional stiffness, monolayer sheets are easily warped out-of-plane, exhibiting ripples,[4,5] folds,[6] and scrolls observed in experiments[7,8] and explored by computational simulation.[9,10] Indeed, one of the salient features of graphene is the sensitivity of electronic properties due to topology,[2,11] resulting in variations in form and functionality. In biology, for example, folding can transform relatively simple molecules into complex shapes with distinct properties.[12,13] The exploration of folded or crumpled geometries in synthetic materials is an active area of research, both theoretically and experimentally.[14–19]

Graphene has a propensity for stable folding—the bending energy at folds is compensated by intersheet adhesion (van der Waals interactions).[10,20] The robust mechanical and electrical properties of graphene combined with such stable folded configurations indicate promise for use in ultracapacitors[21–24] (Fig. 1). Moreover, graphene exhibits an exceptionally high specific surface area (approximately 2675 m^2/g), and the intrinsic capacitance of pristine graphene was found to be 0.21 F/m^2,[25] exceeding the capacitance for all carbon-based materials. To maximize the possible energy storage, the surface area of graphene must be readily accessible by a solution of electrolytes.[21] Here, we explore the configurations of pristine crumpled graphene sheets without any chemical defects, additives, or adsorbents.

II. FOLDING AND FRACTAL DIMENSION

Despite the complicated appearance of crumpled configurations, the folding phenomenon is very robust across many different types of materials and sheet geometries.[15–18,26] Crumpled spheres derived from thin sheets of dimensions $L \times L$ obey a fractal scaling law $\rho_a L^2 \sim R^D$, where $\rho_a = \rho_V h$ is the areal density, h is the thickness (where $h \ll L$), ρ_V is the material mass density, R is the radius of the crumpled sphere, and $2 < D < 3$ is the material-dependent fractal dimension of the crumpled spheres.[27] For sheets without bending rigidity (membranes), the Flory mean-field approximation predicts that the radius of the crumpled balls behaves according to $R \sim \sqrt{\log(L)}$, such that the folded state of self-avoiding sheets exhibit a universal fractal dimension of $D = 2.5$.[28] However, for thin sheets with finite-bending rigidity (such as graphene), the work required to crumple the sheet is governed by the bending and stretching energy stored in the folded creases,[29] and previous investigations suggest a universal value of $D = 2.3$[18] for self-avoiding sheets of fixed thickness. The bending stiffness of monolayer graphene is on the order of 1 to 2 eV (per unit width),[10,30] and thus finite-bending rigidity is assumed. Thus graphene can be considered a thin elastic self-avoiding sheet, where self-adhesion stabilizes folded configurations.

A recent study on adhesive membranes with finite-bending rigidity has shown that while self-adhering sheets (such as graphene) fold during compression as a result of energy minimization, the process at high confinement is similar to crumpling of macroscopic nonadhesive sheets.[19] While forced crumpling of adhesive membranes was investigated with adhesion generated by a vdW-like attractive interaction, sheets were represented by regular elastic lattices with harmonic terms for stretching, bending, and adhesion.[19] To the extent of our knowledge, the behavior and fractal dimension of crumpled graphene has yet to be defined through accurate full atomistic simulations. Accordingly, we investigate the scaling properties of crumpled graphene balls folded from sheets of different sizes L using a molecular dynamics (MD) approach.

It is noted that the thickness (h) of monoatomic structures such as graphene is difficult to define;[31] however, the areal

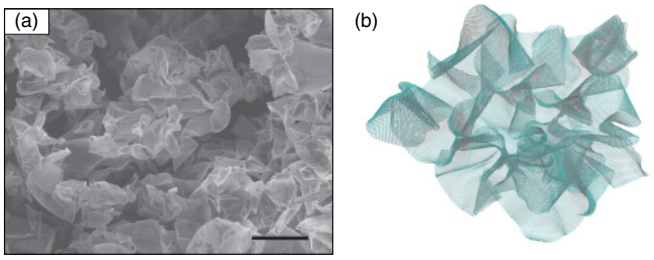

FIG. 1. (Color online) Representations of crumpled graphene. (a) Scanning electron microscopy image of graphene sheets implemented in ultracapacitor (scale bar 10 μm) (from Ref. 21). (b) Full atomistic schematic of crumpled graphene from current investigation. Individual monolayer graphene sheets can be collected and aggregated to fill volume and optimize accessible surface area. Visualization attained by superposition of multiple graphene models in various stages of crumpled deformation (scale bar approximately 10 nm). The folding phenomena at both the nano- and microscales are dependent on the fractal dimension of graphene.

density (ρ_a) can be calculated based on the atomic mass of the constituent carbons. Folding of graphene is not directly analogous to folding of a sheet of paper (an isotropic material without preference for folding axes). In graphene the direction and location of folding lines is influenced by its hexagonal symmetry, and folds along the armchair and zigzag directions are energetically favorable.[20] Even for isotropic elastic sheets, self-avoidance and nonlinear deformations make the crumpling process complex, involving the formation of sharp vertices, cones, and ridges.[32,33] The crumpling phenomena can be viewed as a network of ridges[34]—where formation is a mode of condensation of energy into a small subset of the available volume[29]—similar to the spontaneous organization of dislocations into grain boundaries in a strained crystal.

III. METHODS

Square sheets of graphene (with L_0 from 6 to 20 nm) are simulated atomistically using the adaptive interatomic reactive empirical bond-order (AIREBO) potential for carbon-carbon interactions.[35,36] The AIREBO potential has been shown to provide an accurate account of the chemical and mechanical behavior of hydrocarbons, including graphene.[37,38] Stochastic crumpling the sheets is accomplished by confining the graphene sheets to a spherical domain with a confining spring force (Fig. 2). A time increment is chosen on the order of femtoseconds (0.5×10^{-15} seconds). All MD simulations are subject to a microcanonical (*NVT*) ensemble, carried out at a low temperature (100 K) to minimize thermal fluctuations. Simulations for $L_0 = 8$ nm, 10 nm, 12 nm, 14 nm, and 16 nm were repeated at 300 K to ensure stability at physically relevant temperatures with negligible changes in results. Moreover, recent analysis of the thermal stability of self-adhered membranes indicate that the high stiffness and strong attraction of graphene result in an unbinding temperature of several thousand kelvin, suggesting that folded, scrolled, or crumpled graphene could not be unfold by heating.[19] Temperature control was achieved using a Berendsen thermostat.[39] The

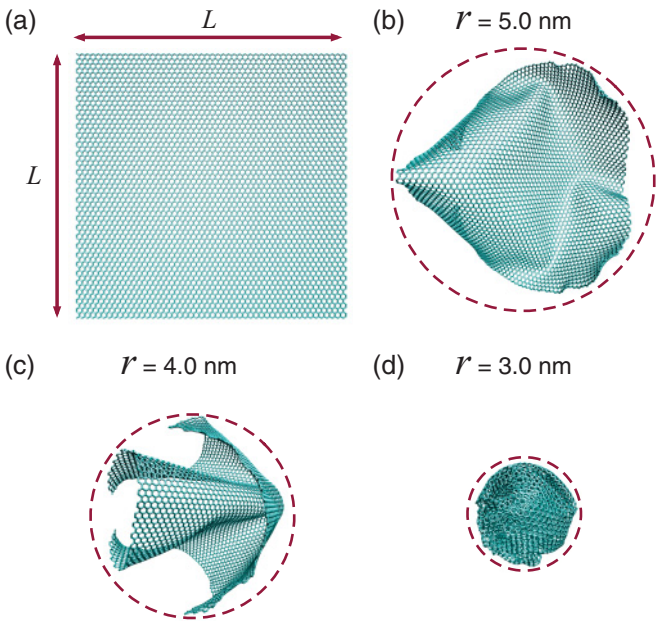

FIG. 2. (Color online) Schematic of stochastic crumpling of graphene. Full atomistic representations of graphene sheets of square dimension $L \times L$ are initially minimized and equilibrated. Crumpling the sheets is accomplished by confining the graphene sheets to a spherical domain with confining spring force, which decreases radius at a constant velocity. Snapshots above depict the crumpling of a 12 nm $\times$ 12 nm sheet, typical of all models. (a) Initial configuration. (b) Crumpling initiated by confining volume; initial deformation characterized by simple out-of-plane warping. (c) Self-folding leads to crumpled configurations with minimal energy expenditure. (d) Final configuration of a dense, spherical ball. Note that here, the depicted geometry is condensed beyond the quasiequilibrium state. Crumpling is carried out until compressive failure occurred.

MD simulations were performed modeling code LAMMPS[40] (http://lammps.sandia.gov/).

Stochastic crumpling the sheets is accomplished by confining the graphene sheets to a spherical domain with a confining spring force $F(r) = K(r - R(t))^2$ for $r > R(t)$, where K is a defined spring constant (0.8 N/m), r is the radial distance of each atoms from the defined center of the spherical domain, and $R(t)$ is the radius of the domain, which is decreased at a constant velocity of 50 m/s. The interaction between the force and graphene is both fricitionless and nonadhesive.

To quantify the available area of crumpled graphene, and the effect of further compression/relaxation on accessible area, the solvent accessible surface area (SASA) is determined assuming water as the electrolyte solution. The SASA[41] of a molecule is the cumulative surface area of the individual atoms that is accessible to a solvent molecule. The atoms and solvent molecule are modeled as spheres using their van der Waals radii, and the SASA is the calculated determination of the percentage of surface exposed to the solvent.[42] For the current study an adapted SASA algorithm is implemented by vmdICE.[43] A radius of 1.4 Å (effective radius of H_2O molecules) is used to represent the electrolyte solution.

For the crumpling phenomena considered here, any potential boundary effects (termination of edge shape) would decrease with the size of the sheet, as the order of folding

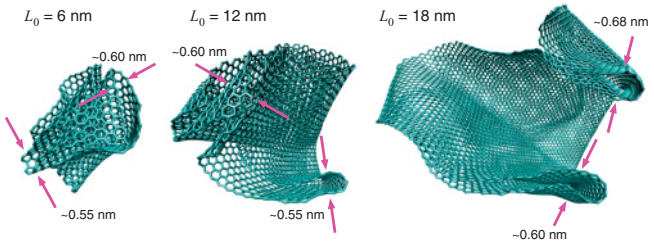

FIG. 3. (Color online) Characteristic scale of crumpled graphene self-folds (sheets with initial length, L_0, of 6, 12, and 18 nm depicted). The length scale of the graphene sheets is chosen as stable self-folding of monolayer graphene, due to the persistence length, occurs on the order of 10 to 20 nm,[10] with a self-fold forming "creases" where the graphene curves about itself. Due to the finite stiffness and self-adhesion, the diameters of these folds are consistently on the order of approximately 0.5 to 0.7 nm, consistent with previous findings of scrolled and racketlike monolayer graphene.[9,10,19] During the crumpling process, arbitrarily large sheets would simply fold and crumple until the folds occur at this scale. This is one advantage of introducing a scale-fee fractal dimension; the resulting crumpled structures are governed by local folding phenomena, so larger models still hold beyond the critical length scale in which stable folding occurs.

events in the bulk—not the edge effects—dominate deformation. Indeed, the edges of the graphene sheets are not terminated with hydrogen atoms. While hydrogen atoms or other termination groups influence the chemical reactivity,[44] test simulations confirmed that termination does not affect the folding and crumpling phenomena. Moreover, the edge shapes of graphene can be armchair, zigzag, or chiral,[45] which defines the electronic properties of graphene at the boundaries.[46,47] However, as the graphene sheet with a hexagonal lattice is considered an isotropic elastic material, the edge shape does not change much of the bulk mechanical properties, especially in the elastic regime and with large radius of curvature in comparison with lattice constants,[48,49] as well as for length scales exceeding approximately 10 nm.[50] The length scale of the graphene sheets is also chosen, as stable self-folding of monolayer graphene, due to the persistence length, occurs on the order of 10 to 20 nm.[10] Inspection of the self-folded geometries of graphene sheets of varying initial lengths depict the formation of "creases" or self-folds with the same characteristic size regardless of initial length (Fig. 3). Due to the finite stiffness and self-adhesion, the diameters of these folds are consistently on the order of approximately 0.5 to 0.7 nm, in agreement with previous findings of scrolled and racketlike monolayer graphene.[9,10,19] During the crumpling process, larger sheets would simply fold and crumple until the folds occur at this scale. In other words lengths on the order of 50 nm or greater can be folded multiple times, but once the scale of the folds and creases is below a length scale of approximately 5–6 nm, they will no longer be stable (unfolding would occur). Moreover, at length scales below 6 nm, the aspect ratio (length, L_0, to commonly presumed effective vdW thickness of graphene, $h = 0.34$ nm) of graphene would deviate from a thin-sheet assumption (where $L/h \approx 20$). The limiting folding dynamics of larger sized sheets would reduce to such scales, and larger model systems are unnecessary. This is one advantage of introducing a scale-fee fractal dimension; the resulting crumpled structures are governed by local folding phenomena, so larger models still hold beyond the critical length scale in which stable folding occurs (approximately 10 to 20 nm).

IV. CRUMPLING OF PRISTINE AND DEFECTIVE GRAPHENE SHEETS

The fractal dimension D relates the size R of a crumpled sheet at a given confinement to its initial size L, where $R \sim L^{2/D}$ and $2 < D < 3$. Thus, D can be thought of as the packing efficiency of the sheet. A value of D close to the lower limit $D = 2$ means a loose packing, whereas a value of D close to the upper limit $D = 3$ means a perfectly ordered compact structure. Order is hindered by the irregular density of vertices, facets, and ridges, and crumpled sheets have $D < 3$. Here, the graphene samples are compressed while tracking the system potential energy (PE). An equilibrium radius (r_{eq}) is defined as the minimum radius in which the gradient of the PE reached zero [Fig. 4(a)]. It is noted that this defines a quasiequilibrium state (local minima) and not the absolute minimum energy of the system. However, such a state can be attained with minimal energetic expense.

It has been shown that the characteristic fractal dimension for any thin sheet material is independent of the bending rigidity.[18,26] The bending stiffness of monolayer graphene is typically calculated assuming beamlike elastic-energy formulations of multilayer graphene. While it is unlikely the crumpled graphene achieves such values presuming beamlike behavior, it has been shown that intersheet shear interactions significantly increase bending stiffness beyond the monolayer value,[51] and thus finite-bending rigidity is maintained. Self-adhesion of graphene facilitates self-folding, effectively decreasing the energy required for crumpling/packing. Strong adhesion allows stable folded structures with minimal energetic requirement. Thus, it is predicted the crumpling behavior of graphene lies somewhere in between an ideal self-avoiding membrane and an ideal sheet with finite rigidity. The combination of variable bending rigidity with self-adhesion results in deviations from the ideal crumpling problem—and an expected increase in fractal dimension. Plotting the logarithm of equilibrium radius (r_{eq}) versus the logarithm of initial length (L_0) yields a linear relation from which the fractal dimension D can be determined [Fig. 4(b)]. A linear regression returns a fractal dimension of $D = 2.358 \pm 0.12$ (R^2 value of 0.987). This lies between an ideal self-avoiding membrane ($D = 2.5$) and an ideal sheet with finite rigidity ($D = 2.3$), suggesting the self-adhesion plays a role in the crumpling of graphene (effectively decreasing the energy required to self-fold/crumple). Note that the quasiequilibrium configurations involve elastic crumpling only, thereby avoiding the effects due to plasticity and applied confining force.[17,26] In addition the fractal dimension is independent of applied boundary conditions (e.g., confining force, load rate, etc.). Stochastic crumpling is actually quite a robust phenomena.[18] If one considers the simple crumpling of a sheet of paper into a ball, regardless of methodology, the ball at the end will have a characteristic shape. We note that although denser packing can be achieved with higher applied force, the relation to fractal dimension is constant.[26]

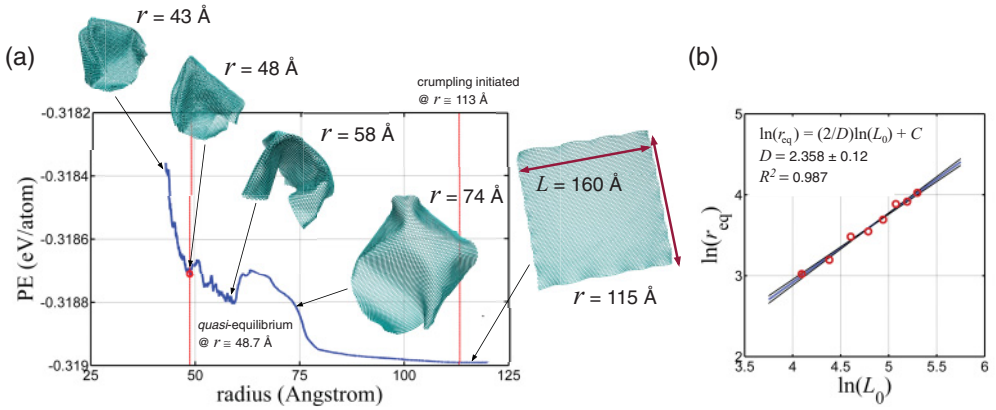

FIG. 4. (Color online) (a) Representative potential energy (PE) profile during crumpling (normalized by atoms) versus radius for sheet with $L_0 = 16$ nm. Crumpling initiated at a radius of approximately 11.3 nm, after which the PE increases due to elastic strain energy. Self-folding begins at a radius of approximately 6 nm, indicated by a sudden decrease of PE due to self-adhesion. Further folding occurs, and a final local minimum is attained at $r = 48.7$ Å, defined as the quasiequilibrium radius (r_{eq}). (b) Via the relation $r \sim L^{2/D}$, the fractal dimension is determined by a linear regression of the logarithm of equilibrium radius (r_{eq}) versus the logarithm of initial length (L_0), where $\ln(r_{eq}) = (2/D)\ln(L_0) + C$. Error of $\pm 2\%$ indicated by diameter of plotted circles. A linear regression returns a slope of 0.848 ± 0.044 resulting in a fractal dimension of $D \cong 2.358 \pm 0.12$ (high and low values also plotted).

The introduction of defects (vacancies) is an intriguing case as it does not fundamentally change the chemical makeup of the material (still pure carbon) while affecting the mechanical behavior of the sheets. Recently, electron irradiation was successfully used to create sp^2-hybridized one-atom-thick flat carbon membranes with a random arrangement,[52] which may open new possibilities for the design and engineering of graphene-based electronic devices. As such, we undertake a systematic investigation of the effect of defect density on the crumpling of graphene. We select the 12 nm × 12 nm graphene sheet to probe the addition of defects, chosen to allow relatively efficient computational times. We introduce random vacancies, ranging from 1% to 15%, and subject the defective sheets to the same crumpling procedure. At high levels of defects, the graphene is more akin to amorphous carbon, attainable in the production of graphene experimentally.[52,53] The transition from randomly "perforated graphene" (point defects) to a 2D coherent amorphous membrane (2D amorphous carbon) greatly affects the crumpling phenomena. We find that the addition of defects reduces the equilibrium crumpled radius, as the inherent rigidity of the graphene sheet is reduced and the sheet can be manipulated into a tighter packed configuration with less carbon [Fig. 5(a)]. As relatively high levels of defects (>10%) are introduced, the graphene sheet can no longer be said to exhibit "membranelike" behavior and essentially acts as a planar collection of amorphous atoms. As such, the process is no longer "crumpling" but merely packing the carbon atoms into a confined spherical volume. The result is that the equilibrium radius approaches that of the theoretical minimum (setting the volume of the initial sheet to an equivalent sphere with equal density, or $V = L_0^2 \times h = (4/3)\pi r_{min}^3$).

V. SOLVENT ACCESSIBLE SURFACE AREA

The fractal dimension suggests a relatively efficient packing of graphene—a disadvantage for use within ultracapacitors. Ultracapacitors can implement electrical double-layer (EDL) capacitance as the energy storage mechanism, requiring a relatively high accessible surface area. Current EDL capacitors contain activated carbon with a high specific surface area as the electrode material, and the capacitance comes from the charge accumulated at the electrode/electrolyte interface. A propensity to self-fold decreases the surface area accessible to electrolyte solution.

The SASA is calculated at the determined equilibrium radius (r_{eq}) for each model. The SASA is then plotted against the initial, ideal surface area of the graphene, where $A_0 = 2 \times L_0^2$ [Fig. 6(a)]. A linear regression is calculated with a fitted ratio of $dA_{SASA}/dA_0 = 0.586$ ($R^2 = 0.984$). Thus, at crumpled equilibrium, approximately 58.6% of the accessible surface area is maintained. Taking the specific

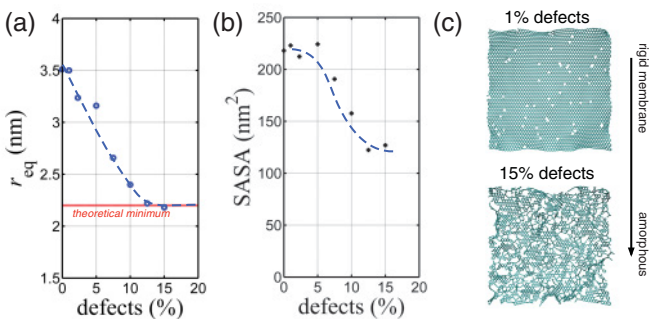

FIG. 5. (Color online) Effect of vacancy defects. Plots depict results of crumpling defective graphene sheets with $L_0 = 12$ nm, defects from 0% to 15%. (a) Equilibrium radius as a function of defects, depicting decrease in radius with increase in defect density. (b) SASA as a function of defect density. (c) Representative schematics of defective graphene depicting transition from rigid membrane-like graphene sheets with point defects to planar amorphous carbon.[52] Dashed lines intended as visual guide only.

surface area of graphene as 2675 m^2/g[21] and the intrinsic capacitance of graphene as 0.21 F/m^2,[21,25] we can calculate the upper limit of EDL capacitance for freely crumpled graphene, determined to be approximately 329 F/g. Recently, it has been demonstrated that graphene-based ultracapacitors have high specific capacitance in the range of 135 to 264 F/g.[22,54,55]

We note that our intent here is to explore the variation in accessible surface area upon crumpling graphene sheets and not the determination of the electronic properties of such systems *per se*. As such, we do not infer that the measured capacitance of pristine and planar graphene is constant under changes in topography of induced defects. The variation in electronic properties of deformed or defective graphene requires quantum-level investigations that are beyond the scope of the mechanistic MD implemented here. Experimental and *ab initio* investigations include the introduction of defects to manipulate charge carrier concentrations,[2,56] the influence of out-of-plane deformation (i.e., curvature) of electronic properties,[11] tunable bandgaps via chemical doping,[57] or the variation in band structure for graphene mono-, bi-, and trilayers,[58] which would naturally appear in a sufficiently crumpled graphene system. However, it has been previously demonstrated that the exploitation of deformed or curved graphene has practical applications in ultracapacitors and serve to increase the attained levels of electrolyte contact.[21] Here, we relate the accessible area (SASA) to capacitance via a simple scaling relation, assuming an ideal constant value of specific capacitance. Moreover, due to the uncertainties in the experimental samples and measurement, as well as the fact our value is obtained by freely crumpled graphene without solvent, a decrease from the values predicted here is expected. As a comparison, untreated pristine carbon nanotubes exhibit experimentally measured capacitance in the range of approximate 50 to 200 F/g.[59–61] While this capacitance can potentially be increased by chemical functionalization or electrolyte type, it is often to the detriment of cyclability.[62]

The plot reflects the calculated specific SASA (m^2/g) versus radius for all models [Fig. 6(b)]. We note that the initial SASA for all models exceeds the specific surface area of graphene (2675 m^2/g), as the calculation considers the exterior edges of the graphene sheets as accessible area. At equilibrium, we find an average specific SASA of 1590 ± 217.2 m^2/g. Converting to capacitance results in 329 ± 45.6 F/g. While the crumpling process is stochastic, we also note a near-linear decrease in specific SASA once crumpling is initiated. We also determine the dynamic SASA as a function of radius [Fig. 6(b)] to indicate the affect of further compression/relaxation on accessible area. The plot reflects the calculated specific SASA (m^2/g) versus radius for all models. Through linear regressions we determine the change in specific SASA with respect to a change in radius to be approximately 710 ± 280 m^2/g per nanometer or 149.1 ± 58.8 F/g per nanometer. Thus, once crumpled, the achievable capacitance is highly dependent on confined volume, with significant decreases with marginal decrease in volume. For example, a graphene sheet with an initial dimension of $L_0 = 12$ nm will have an ideal capacitance of ≈470 F/g when confined by a sphere of radius 4.5 nm and only ≈221 F/g at a radius of 2.5 nm. Moreover, we find that the addition of defects also reduces the SASA, as the less rigid graphene is more tightly packed [Fig. 5(b)]. While the introduction of defects has been shown to marginally affect capacitance through irradiation, the defect density is relatively low.[63] Moreover, amorphous carbon has been shown to have an intrinsic capacitance less than graphene.[64]

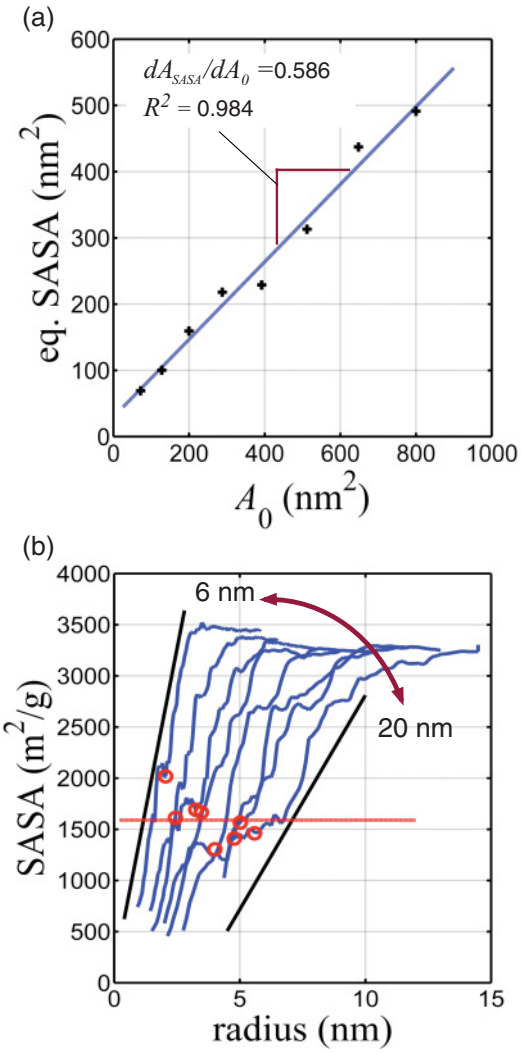

FIG. 6. (Color online) Equilibrium and evolution of solvent accessible surface area (SASA). (a) SASA of crumpled graphene at equilibrium (e.g., SASA) plotted against the initial surface area A_0. Fitted ratio of $dA_{SASA}/dA_0 = 0.586$ ($R^2 = 0.984$) is shown. (b) Specific SASA (m^2/g) as a function of contracting confining radius (nm); equilibrium values indicated by red circles. At equilibrium, we find an average specific SASA of 1590 ± 217.2 m^2/g. By linear regression, we determine the change in specific SASA with respect to a change in radius to be approximately 710 ± 280 m^2/g per nanometer (upper and lower fits shown).

VI. VARIATION IN ADHESION ENERGY

The propensity to self-fold is disadvantageous to the use in ultracapacitors, as adjacent sheets stick to each other preventing electrolyte contact. Moreover, the self-attraction of graphene differentiates the crumpling of graphene from crumpling of paper. As such, a theoretical variation in the adhesion strength is investigated to determine the effect of

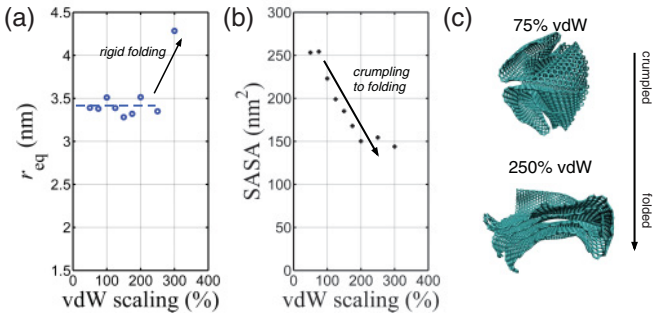

FIG. 7. (Color online) Effect of adhesion energy (scaling van der Waals). Plots depict results of crumpling graphene sheets ($L_0 =$ 12 nm) with variation in vdW adhesion from 50% to 300% initial value. (a) Equilibrium radius as a function of vdW adhesion, depicting nominal changes (r_{eq} ranging from 3.32 to 3.51 nm for 50% to 250% vdW adhesion). At 300% vdW adhesion, the sheet undergoes strong self-folding, and the rigid assembly fails under further compression. (b) SASA as a function of vdW adhesion, indicating constant decrease in area with an increase in self-adherence. (c) Schematics depicting crumpling (75% vdW) to self-folding dominant deformation (250% vdW).

self-attraction. A set of simulations is performed with varying adhesion strength by scaling the vdW adhesion from 50% to 300% the original value in the AIREBO potential and $L_0 =$ 12 nm is again selected as a model system.

We find that, for variations in vdW adhesion, there is nominal change in the equilibrium radius up to 250% the initial value [r_{eq} ranging from 3.32 to 3.51 nm; Fig. 7(a)]. We note that substituting any of these values would not affect the calculated fractal dimension of $D \approx 2.36$. For 300% vdW adhesion, there is an abrupt change—the graphene undergoes extreme self-folding and, upon compression, fails. Analysis of the accessible surface reveals a more consistent transition, where an increase in the vdW adhesion causes a steady decrease in the accessible area [Fig. 7(b)]. Rather than crumple, the graphene is more likely to self-fold and self-adhere, eliminating any surfaces for electrolyte contact. For example, while 50% vdW and 250% vdW can be confined to roughly same equilibrium volume, the former has approximately 1.6 the effective SASA. While self-adhesion can be said to (nominally) increase the fractal dimension and effective packing of crumpled graphene, it is detrimental to the accessible surface area. As such, the nominal attraction provided by vdW interaction is both necessary to induce stable crumpled structures and weak enough to allow accessible surface area.

VII. SUMMARY

In sum, here we investigated the packing efficiency and accessible surface area of crumple monolayer graphene to estimate the achievable capacitance of graphene-based ultracapacitors. By simple crumpling simulations of graphene sheets of various dimensions, we have determined the fractal dimension to be $D = 2.36 \pm 0.12$. This is higher than the theoretical value for an ideal elastic sheet with bending rigidity ($D = 2.3$), indicating the self-adhesion of monolayer graphene facilitates a denser packing arrangement. The SASA is calculated for crumpled configurations, and relating the crumpled geometry to the specific capacitance, we predict an average, idealized specific capacitance of 329 ± 45.6 F/g for crumpled graphene, highly dependent on the confining volume. Graphene offers a unique platform to explore crumpling due to the existence of defects and self-adhesion properties. In general the addition of defects allows tighter packing of crumpled graphene through a decrease in structural rigidity, but it also decreases the SASA due to more efficient packing. Similarly, an increase in vdW adhesion results in self-adherence and a subsequent decrease in SASA due to a transition to folding dominated deformation. We conclude that, for application in ultracapacitors, pristine graphene with relatively weak vdW adhesion is optimal. The addition of chemical absorbents could affect the inherent capacitance of the graphene,[65–67] but the focus of the study reported here is to provide a means of comparison, with pristine graphene providing a baseline for such impure systems. As it is presumed the entire surface area of graphene will never by accessible for ultracapacitor applications, the simple crumpling simulations carried out here delineate a range of attainable values and sets a theoretical upper bound for crumple graphene capacitance. Such an approach could potentially be implemented for the behavior of graphene flakes in solution[53,68] or other ultracapacitor systems such as graphene oxide[55] or graphene/polymer[67] composites.

ACKNOWLEDGMENTS

This work was supported primarily by the MRSEC Program of the National Science Foundation (Award No. DMR-0819762) with additional support from the ARO-MURI program (Award No. W911NF-09-1-0541). Visualization was carried out using Visual Molecular Dynamics.[69]

*mbuehler@mit.edu

[1] C. Lee, X. Wei, J. Kysar, and J. Hone, Science **321**, 385 (2008).
[2] A. H. Castro Neto, F. Guinea, N. M. R. Peres, K. S. Novoselov, and A. K. Geim, Rev. Mod. Phys. **81**, 109 (2009).
[3] S. Stankovich, D. A. Dikin, G. H. B. Dommett, K. M. Kohlhaas, E. J. Zimney, E. A. Stach, R. D. Piner, S. T. Nguyen, and R. S. Ruoff, Nature **442**, 282 (2006).
[4] A. Fasolino, J. H. Los, and M. I. Katsnelson, Nat. Mater. **6**, 858 (2007).
[5] W. Z. Bao, F. Miao, Z. Chen, H. Zhang, W. Y. Jang, C. Dames, and C. N. Lau, Nature Nanotechnology **4**, 562 (2009).
[6] K. Kim, Z. Lee, B. D. Malone, K. T. Chan, B. Alemán, W. Regan, W. Gannett, M. F. Crommie, M. L. Cohen, and A. Zettl, Phys. Rev. B **83**, 245433 (2011).
[7] J. C. Meyer, A. K. Geim, M. I. Katsnelson, K. S. Novoselov, T. J. Booth, and S. Roth, Nature **446**, 60 (2007).
[8] R. B. Kaner, L. M. Viculis, and J. J. Mack, Science **299**, 1361 (2003).
[9] X. Shi, N. M. Pugno, and H. Gao, Journal of Computational and Theoretical Nanoscience **7**, 1 (2010).
[10] S. Cranford, D. Sen, and M. J. Buehler, Appl. Phys. Lett. **95**, 123121 (2009).

[11]P. Wu, J. Zhang, and K. P. Ong, J. Phys. Chem. C **114**, 12749 (2010).
[12]C. M. Dobson, Nature **426**, 884 (2003).
[13]J. U. Bowie, Nature **438**, 581 (2005).
[14]E. Cerda and L. Mahadevan, Phys. Rev. Lett. **90**, 074302 (2003).
[15]K. Matan, R. B. Williams, T. A. Witten, and S. R. Nagel, Phys. Rev. Lett. **88**, 076101 (2002).
[16]A. S. Balankin and O. S. Huerta, Phys. Rev. E **77**, 051124 (2008).
[17]T. Tallinen, J. A. Astrom, and J. Timonen, Nat. Mater. **8**, 25 (2009).
[18]G. A. Vliegenthart and G. Gompper, Nat. Mater. **5**, 216 (2006).
[19]T. Tallinen, J. A. Astrom, P. Kekalainen, and J. Timonen, Phys. Rev. Lett. **105**, 026103 (2010).
[20]J. Zhang, J. L. Xiao, X. H. Meng, C. Monroe, Y. G. Huang, and J. M. Zuo, Phys. Rev. Lett. **104**, 166805 (2010).
[21]C. G. Liu, Z. N. Yu, D. Neff, A. Zhamu, and B. Z. Jang, Nano Lett. **10**, 4863 (2010).
[22]M. D. Stoller, S. J. Park, Y. W. Zhu, J. H. An, and R. S. Ruoff, Nano Lett. **8**, 3498 (2008).
[23]Y. Wang, Z. Q. Shi, Y. Huang, Y. F. Ma, C. Y. Wang, M. M. Chen, and Y. S. Chen, J. Phys. Chem. C **113**, 13103 (2009).
[24]L. L. Zhang, R. Zhou, and X. S. Zhao, J. Mater. Chem. **20**, 5983 (2010).
[25]J. L. Xia, F. Chen, J. H. Li, and N. J. Tao, Nature Nanotechnology **4**, 505 (2009).
[26]A. S. Balankin, I. C. Silva, O. A. Martinez, and O. S. Huerta, Phys. Rev. E **75**, 051117 (2007).
[27]M. A. F. Gomes, Am. J. Phys. **55**, 649 (1987).
[28]Y. Kantor, M. Kardar, and D. R. Nelson, Phys. Rev. A **35**, 3056 (1987).
[29]A. Lobkovsky, S. Gentges, H. Li, D. Morse, and T. A. Witten, Science **270**, 1482 (1995).
[30]Q. Lu, M. Arroyo, and R. Huang, J. Phys. D: Appl. Phys. **42**, 102002 (2009).
[31]Y. Huang, J. Wu, and K. C. Hwang, Phys. Rev. B **74**, 245413 (2006).
[32]T. Liang and T. A. Witten, Phys. Rev. E **71**, 016612 (2005).
[33]B. A. DiDonna and T. A. Witten, Phys. Rev. Lett. **8720**, 206105 (2001).
[34]E. M. Kramer and T. A. Witten, Phys. Rev. Lett. **78**, 1303 (1997).
[35]D. W. Brenner, O. A. Shenderova, J. A. Harrison, S. J. Stuart, B. Ni, and S. B. Sinnott, J. Phys. Condens. Matter **14**, 783 (2002).
[36]S. J. Stuart, A. B. Tutein, and J. A. Harrison, J. Chem. Phys. **112**, 6472 (2000).
[37]Z. P. Xu and M. J. Buehler, Nanotechnology **20**, 185701 (2009).
[38]C. D. Reddy, A. Ramasubramaniam, V. B. Shenoy, and Y. W. Zhang, Appl. Phys. Lett. **94**, 101904 (2009).
[39]H. J. C. Berendsen, J. P. M. Postma, W. F. Vangunsteren, A. Dinola, and J. R. Haak, J. Chem. Phys. **81**, 3684 (1984).
[40]S. J. Plimpton, J. Comput. Phys. **117**, 1 (1995).
[41]B. Lee and F. M. Richards, J. Mol. Biol. **55**, 379 (1971).
[42]A. Shrake and J. A. Rupley, J. Mol. Biol. **79**, 351 (1973).
[43]B. Knapp, N. Lederer, U. Omasits, and W. Schreiner, J. Comput. Chem. **31**, 2868 (2010).
[44]O. Hod, V. Barone, J. E. Peralta, and G. E. Scuseria, Nano Lett. **7**, 2295 (2007).
[45]X. Jia, M. Hofmann, V. Meunier, B. G. Sumpter, J. Campos-Delgado, J. M. Romo-Herrera, H. Son, Y.-P. Hsieh, A. Reina, J. Kong, M. Terrones, and M. S. Dresselhaus, Science **323**, 1701 (2009).
[46]Y. W. Son, M. L. Cohen, and S. G. Louie, Phys. Rev. Lett. **97**, 216803 (2006).
[47]Z. P. Xu, Q. S. Zheng, and G. H. Chen, Appl. Phys. Lett. **90**, (2007).
[48]N. R. Aluru, H. Zhao, and K. Min, Nano Lett. **9**, 3012 (2009).
[49]Z. P. Xu, Journal of Computational and Theoretical Nanoscience **6**, 625 (2009).
[50]Q. Lu, W. Gao, and R. Huang, Modell. Simul. Mater. Sci. Eng. **19**, 054006 (2011).
[51]Y. Liu, Z. Xu, and Q. Zheng, J. Mech. Phys. Solids **59**, 1613 (2011).
[52]J. Kotakoski, A. V. Krasheninnikov, U. Kaiser, and J. C. Meyer, Phys. Rev. Lett. **106**, 105505 (2011).
[53]K. A. Mkhoyan, K. H. Liao, A. Mittal, S. Bose, C. Leighton, and C. W. Macosko, ACS Nano **5**, 1253 (2011).
[54]X. A. Du, P. Guo, H. H. Song, and X. H. Chen, Electrochim. Acta **55**, 4812 (2010).
[55]Y. W. Zhu, S. Murali, M. D. Stoller, A. Velamakanni, R. D. Piner, and R. S. Ruoff, Carbon **48**, 2118 (2010).
[56]J. Lahiri, Y. Lin, P. Bozkurt, I. I. Oleynik, and M. Batzill, Nature Nanotechnology **5**, 326 (2010).
[57]E. Rotenberg, T. Ohta, A. Bostwick, T. Seyller, and K. Horn, Science **313**, 951 (2006).
[58]P. Jarillo-Herrero, T. Taychatanapat, K. Watanabe, and T. Taniguchi, Nat. Phys. **7**, 621 (2011).
[59]C. M. Niu, E. K. Sichel, R. Hoch, D. Moy, and H. Tennent, Appl. Phys. Lett. **70**, 1480 (1997).
[60]K. H. An, W. S. Kim, Y. S. Park, J. M. Moon, D. J. Bae, S. C. Lim, Y. S. Lee, and Y. H. Lee, Adv. Funct. Mater. **11**, 387 (2001).
[61]R. Signorelli, D. C. Ku, J. G. Kassakian, and J. E. Schindall, Proc. IEEE **97**, 1837 (2009).
[62]P. Simon and Y. Gogotsi, Nat. Mater. **7**, 845 (2008).
[63]S. Sonde, F. Giannazzo, V. Raineri, and E. Rimini, Phys. Status Solidi B **247**, 907 (2010).
[64]M. Ramani, B. S. Haran, R. E. White, B. N. Popov, and L. Arsov, J. Power Sources **93**, 209 (2001).
[65]K. G. Tabrizi and R. Majidi, Fullerenes Nanotubes and Carbon Nanostructures **19**, 532 (2011).
[66]T. B. Martins, R. H. Miwa, A. J. R. da Silva, and A. Fazzio, Phys. Rev. Lett. **98**, 196803 (2007).
[67]Q. Wu, Y. X. Xu, Z. Y. Yao, A. R. Liu, and G. Q. Shi, ACS Nano **4**, 1963 (2010).
[68]Y. Hernandez, V. Nicolosi, M. Lotya, F. M. Blighe, Z. Sun, S. De, I. T. McGovern, B. Holland, M. Byrne, Y. K. Gun'ko, J. J. Boland, P. Niraj, G. Duesberg, S. Krishnamurthy, R. Goodhue, J. Hutchison, V. Scardaci, A. C. Ferrari, and J. N. Coleman, Nature Nanotechnology **3**, 563 (2008).
[69]W. Humphrey, A. Dalke, and K. Schulten, J. Mol. Graphics **14**, 33 (1996).